

# Dirty Fireballs and Orphan Afterglows: A Tale of Two Transients

James E. Rhoads <sup>1</sup>

## ABSTRACT

Orphan afterglows are transient events that are produced by cosmological fireballs and resemble gamma ray burst (GRB) afterglows, yet are not accompanied by gamma rays. Such transients may be produced by jetlike GRBs observed off-axis, and therefore hold great promise as a test of gamma ray burst collimation. However, orphans may also be produced by “dirty fireballs,” i.e., cosmological fireballs whose ejecta carry too many baryons to produce a GRB.

A well designed orphan afterglow search can distinguish between on-axis dirty fireballs and off-axis orphans in at least two ways. First, by combining real-time triggers from a wide area, multicolor search with deeper followup observations, the light curve can be tracked for a time  $\gtrsim 2t_1$ , where  $t_1$  is the age of the event at first observation. Such a light curve allows simultaneous fits to  $t_1$  and the time decay slope  $\alpha$  with sufficient accuracy to distinguish on- and off-axis orphans. Second, radio followup of orphan afterglows will show whether the radio flux is falling in time (as expected for an off-axis orphan) or not (as expected for on-axis events). Additional tests involving multi-band monitoring of the cooling, self-absorption, and  $f_\nu$  peak frequencies are also possible, although much more observationally demanding.

A further complication in orphan searches is that dirty fireballs are likely to *also* be collimated, and that collimated dirty fireballs viewed off-axis will individually be practically indistinguishable from off-axis GRB afterglows. To recognize their presence, orphan afterglow surveys must be sufficiently extensive to catch at least some dirty fireballs on-axis.

*Subject headings:* gamma rays—bursts

## 1. Introduction

Orphan afterglows offer great potential as a test of gamma ray burst collimation (Rhoads 1997). An orphan afterglow is (conventionally) a collimated gamma ray burst viewed far enough from the jet axis that no gamma rays are observed but close enough to the axis that longer wavelength and less tightly collimated afterglow radiation is observed. The properties of such orphans should be similar to the properties of on-axis afterglows viewed at late times, after the light curve break

---

<sup>1</sup>Space Telescope Science Institute, 3700 San Martin Drive, Baltimore, MD 21218

expected in collimated GRB afterglows (Rhoads 1999). Details of the expected orphan afterglow count rate depend substantially on details of the assumed GRB population. Pessimistic numbers result if the kinetic energy in the GRB ejecta is assumed to scale with jet solid angle (Dalal, Griest, & Pruet 2002). Fortunately, present evidence suggests that the burst energy is approximately independent of collimation angle (Frail et al 2001; Panaitescu & Kumar 2002). In this case, an afterglow will be detectable to an off-axis angle that is independent of the initial jet angle, and the orphan afterglow rate can greatly exceed the GRB rate and provide a strong diagnostic of collimation (Granot et al 2002; Totani & Panaitescu 2002; Nakar, Piran, & Granot 2002 [NPG02]).

However, transients resembling GRB afterglows can also be produced by cosmological explosions that do not produce gamma ray bursts. Afterglow emission at any particular frequency reaches peak intensity at some characteristic time and characteristic Lorentz factor  $\Gamma_a$  of the burst ejecta. The observed behavior is essentially independent of the initial Lorentz factor  $\Gamma_0$  of the explosion provided that  $\Gamma_0 > \Gamma_a$ . Optical depth arguments require  $\Gamma_0 \gtrsim 100$  to produce the observed power law GRB spectra (Paczynski 1986; Goodman 1986; Krolik & Pier 1991; Woods & Loeb 1995.) Fireballs with  $10 \lesssim \Gamma_0 \ll 100$  will not produce detectable gamma ray emission but will still produce detectable afterglows at radio, optical, and (if  $\Gamma_0$  is large enough) X-ray wavelengths.

Thus, dirty fireballs can produce transients with the generic characteristics of GRB afterglows, i.e., broken power law spectra and light curves produced by synchrotron emission in a forward external shock. Rhoads (2000) remarked on this possibility and suggested that the difference in light curves could be used to distinguish the two. The principle here is that afterglows from jetlike bursts seen off-axis at frequencies above the peak in  $f_\nu$  will show a rapid decay  $f_\nu \propto t^{-p}$  (where  $p$  is the electron energy distribution power law index). In contrast, afterglows from dirty fireballs will show a much slower decay,  $f_\nu \propto t^{-3(p-1)/4}$  or  $t^{1/2-3p/4}$  (depending on whether the cooling frequency  $\nu_c$  lies above or below the observed frequency).

Huang, Dai, & Lu (2002; hereafter HDL02) examined the requirements for distinguishing orphan afterglows due to off-axis jets from those due to dirty fireballs (which they term “failed gamma-ray bursts” or “FGRBS”). They point out that a major difficulty in distinguishing the two is the unknown trigger time. In studies of triggered GRBs, the decay index  $\alpha$  can be determined without ambiguity using the arrival time of the first gamma rays as the time origin  $t_0$ . (A modest exception can be made for GRB 990123, where the availability of optical ROTSE data during the GRB itself [Akerlof et al 1999] introduces some sensitivity of the early decay index to the precise choice of the time origin.) However, in an orphan afterglow, the trigger time is unknown. All we know is the discovery time  $t_d$ . The age of the burst at discovery can be defined as  $t_1 \equiv t_d - t_0$  and becomes parameter of the light curve that we may try to fit. In general, there is a substantial degeneracy between  $\alpha$  and  $t_1$  unless the observations span a period of duration  $\Delta t \gtrsim 2t_1$ . HDL02 suggest a few tests that might help discriminate dirty fireballs from off-axis GRBs, but conclude that the only promising one is the possibility (unconfirmed at present) that most dirty fireballs are accompanied by “x-ray flashes” of the type observed by the BeppoSAX (e.g., Heise et al 2001) and HETE-II satellites.

In this paper, I point out that dirty fireballs observed on-axis may be identified in orphan afterglow searches through their multiwavelength properties. By using quantities whose evolution changes sign at the jet break, we obtain tests that are robust to the uncertainty in  $t_1$ . Additionally, I examine the distribution of  $t_1$  expected under a simple orphan afterglow search strategy, in order to constrain the typical monitoring period  $\Delta t$  required to reliably fit both  $t_1$  and  $\alpha$ .

## 2. Multiwavelength Monitoring as a Diagnostic of Dirty Fireballs

In simple models, an afterglow is characterized by three spectral break frequencies and a peak flux density (Sari, Piran, & Narayan 1998). The breaks are  $\nu_m$ , corresponding to the observed peak of synchrotron emission for the minimum energy of the electron power law distribution;  $\nu_c$ , corresponding to the observed peak of synchrotron emission for electrons whose cooling time equals the dynamical age of the remnant; and  $\nu_a$ , the synchrotron self-absorption frequency. The spectral peak is  $f_{\nu,m} \equiv f_\nu(\nu_m)$ . An afterglow model predicts the evolution of each of these quantities in terms of physical quantities that control the fireball evolution and emission: The initial energy  $E_0$ , the ambient density  $n = \rho/(\mu m_p)$ , and the fractions of the total available energy converted into relativistic electrons  $\xi_e$  and into magnetic fields  $\xi_b$  at the forward shock of the expanding blast wave. Common generalizations include nonspherical explosions, with initial opening angle  $\zeta$ , and a nonuniform ambient medium, with density  $n \propto r^{-\delta}$ . (Usually, either  $\delta = 0$  for a uniform medium or  $\delta = 2$  as expected for a constant velocity wind from the GRB progenitor).

The light curve of an afterglow depends on the time evolution of the spectrum in a way that depends on the details of the model (e.g., spherical or collimated flow, uniform or wind medium) but in all cases samples only a fraction of the full information provided by the multifrequency behavior of the transient. Thus, when HDL02 examined the possibilities for distinguishing dirty fireballs from off-axis jets primarily using the light curve at a single observed frequency, they used a subset of the available tools and reached unduly pessimistic conclusions.

Consider a quantity  $x$  that behaves as a power law of the time elapsed since the burst,  $x \propto (t - t_0)^q$ . Following HDL02, suppose we do not know  $t_0$  but have made a guess  $t_0^{obs} = t_0 + T$  that is in error by amount  $T$ . Then  $x \propto (t - (t_0^{obs} - T))^q$ . Without loss of generality, we can set the origin of time to the assumed burst trigger,  $t_0^{obs} = 0$ , simplifying the previous expression to  $x \propto (t + T)^q$ . Then the instantaneous slope measurement becomes  $q^{obs}(t) \equiv d \log x / d \log(t) = qt / (t + T)$ . While our measurement of  $q$  will be substantially in error unless  $|T|/t \ll 1$ , we see that the sign of  $q^{obs}$  is unaffected. (Note that  $(t + T)$  is always positive, since our first observation cannot precede the actual trigger time.)

We should therefore measure the behavior of one or more quantities whose sign changes at the transition from effectively spherical to effectively jetlike behavior. Table 1 lists several potentially applicable quantities, together with their expected evolution after the jet break and before the break in either a uniform density ambient medium or a wind environment. Spherically symmetric GRB

remnants expanding into a wind density profile  $\rho \propto r^{-2}$  are more similar to jetlike afterglows than are their uniform density counterparts in terms of several observables (peak flux density, absorption frequency, and fixed frequency light curves).

The most promising observable is the radio light curve, for two reasons. First, the radio flux falls with time after a jet break, while it remains flat or rises prior to a jet break for any likely density profile. Second, it is the simplest to observe, requiring data at only one frequency.

Combinations of the remaining diagnostics can be used similarly to distinguish among the three broad model classes in table 1. In particular, the cooling frequency  $\nu_c$  can be combined with the spectral peak  $f_{\nu,m}$ . If  $f_{\nu,m}$  is declining with time, it indicates either a wind-like ambient medium or a post-break jet. In the first case,  $\nu_c$  should rise with time, while in the second case  $\nu_c$  should remain steady. The self-absorption frequency  $\nu_a$  could substitute for  $f_{\nu,m}$  in this argument, though its time dependence is weaker than that of  $f_{\nu,m}$ . These two-diagnostic tests will be observationally challenging, because the observations involved require good measurements over a wide wavelength range and because it may be hard to distinguish between a truly non-evolving  $\nu_c$  and a relatively weak evolution in an old orphan afterglow. Thus, we tend to prefer either the radio light curve or a suitably detailed optical/IR light curve (section 3) for their conceptual and observational simplicity.

### 3. Two-parameter Fitting of Optical Orphan Light Curves

Even in the case where multiwavelength data are not available, the nature of an optically discovered orphan may be determined by sufficiently accurate monitoring observations. There are three relevant adjustable parameters of the monitoring strategy: Time sampling  $\delta t$ , number of epochs observed  $N$ , and photometric accuracy. We will presume in this section a monitoring strategy where a wide-field survey camera of moderate sensitivity is used to find orphan afterglow candidates, with each epoch of data processed in a time  $\ll \delta t$ . The search strategy should employ multiple optical filters spanning the Balmer break, so that color information can be used to identify the best orphan afterglow candidates in a single epoch (Rhoads 2001). Candidates thus found could then be followed up by larger telescopes. We will therefore presume that the fractional uncertainty in flux measurements is constant throughout the monitoring campaign. We will write this accuracy in magnitudes,  $\delta m = \delta(2.5 \log_{10} f) \approx 1.0857(\delta f)/f$ , where  $f$  and  $\delta f$  are the flux and its associated uncertainty in linear units.

We now ask what kind of observational strategies will be sufficient to distinguish the light curves of an off-axis orphan afterglow and an on-axis dirty fireball. Assume that we either obtained the spectral slope  $\beta$  of the transient already (since our initial search exploits color information) or else will obtain it during the followup campaign. Further, assume that we can deredden the measured spectral slope moderately well using its observed spectral curvature. (This is not trivial, but the required accuracy is not high.) Then we can infer the expected light curve slopes under either of two possible regimes. If the observations are above the cooling frequency for the burst,

Table 1. Indicators of Orphan Afterglow Origins

Quantity	Conditions:		
	$t < t_{jet}$ uniform	$t < t_{jet}$ wind	$t > t_{jet}$
$f_{\nu,m}$	0	-1/2	-1
$\nu_c$	-1/2	+1/2	0
$\nu_a$	0	-3/5	-1/5
$f_{radio}^a$	1/2	0	-1/3

<sup>a</sup>“ $f_{radio}$ ” is here defined as the flux density for frequencies  $\nu$  such that  $\nu_a < \nu < \nu_m$ . This corresponds to cm-wave and mm-wave radio frequencies for typical GRB afterglows.

Note. — Power law exponents for the time evolution of afterglow emission parameters. Each line of the table lists a physical quantity “ $x$ ” (in the first column) followed by its time evolution exponents  $q$  (defined as  $x \propto t^q$ ) in three different evolution regimes. Columns 2 and 3 are both for an on-axis afterglow viewed before the jet break time, which corresponds to the early time regime for conventional GRB afterglows and dirty fireballs. Column 2 is for a uniform ambient density and column 3 for  $\rho \propto r^{-2}$  (as expected if the ambient medium is a steady wind from the GRB progenitor). Column 4 is for the evolution after the jet break (independent of ambient density profile; see Chevalier & Li 1999), and so illustrates the full observable evolution of an orphan afterglow from an off-axis jet. These physical parameters were chosen because they change sign at  $t \approx t_{jet}$ , at least for some ambient density laws. They therefore provide robust tests of whether an observed orphan afterglow is due to an off-axis event or an on-axis “dirty fireball.” The tabulated time evolution slopes are taken from Rhoads (1999), Chevalier & Li (1999, 2000), and Sari, Piran, & Halpern (1999).

the electron spectral slope index  $p$  is given by  $p = 2\beta$  and the time decay slope is either  $p = 2\beta$  (for an off-axis orphan) or  $3p/4 - 1/2 = 3\beta/2 - 1/2$  (for an on-axis dirty fireball). On the other hand, if the observations are below the cooling frequency, we have  $p = 2\beta + 1$  and decay slopes of either  $p = 2\beta + 1$  or  $3p/4 - 3/4 = 3\beta/2$ . To distinguish the two afterglow regimes, we therefore need to tell apart two time decay slopes  $\alpha$  differing by either  $p/4 + 1/2 = \beta/2 + 1/2$  or by  $p/4 + 3/4 = \beta/2 + 1$ . Since  $p \approx 2$  is typical we will be satisfied with any observational strategy that can measure  $\alpha$  to a one-sigma accuracy of  $\pm 0.3$ , sufficient to distinguish the above two scenarios at a  $3\sigma$  level.

To determine the error in  $\alpha$ , I have generated artificial power law light curves sampled according to an assumed observing strategy and with artificial noise added. I then fit each simulated light curve with a model  $f = f_1[(\hat{t} + t_1)/t_1]^{-\alpha}$ , where  $\hat{t}$  is the time elapsed since the first observation. The first numerical experiments were used to demonstrate that the accuracy of the recovered spectral slope  $\alpha_{obs}$  does not vary substantially with the intrinsic slope  $\alpha$  over the range  $1 \lesssim \alpha \lesssim 3$  for a wide range of observing strategies. The remaining simulations therefore used a uniform value of  $\alpha = 1.8$ , near the midpoint of the interesting range.

Because we model the light curves to be power law decays after the first detection at time  $t_1$ , there is only one characteristic timescale in the light curve ( $t_1$ ). Only the ratio  $\delta t/t_1$  need be considered in studying the accuracy of light curve fitting. I have therefore fixed  $\delta t = 1$  day in the simulations while allowing  $t_1$  to vary. Results for  $\delta t = k$  days can be inferred by replacing  $t_1$  with  $t_1/k$  in the figures.

Figure 1 shows how the uncertainty in  $\alpha$  varies with photometric accuracy, for a baseline strategy of nightly samples ( $\delta t = 1$  day) continued for 7 nights total and for  $t_1 = 0.5, 1, 2$  days.

Figure 2 shows the variation of  $\delta\alpha$  with the total duration  $\Delta t = (N - 1)\delta t$  of monitoring, for the two cases where we (a) fix  $\delta t/t_1 = 1$  and vary  $N$ , and (b) fix  $N = 7$  and vary  $\delta t/t_1$ . The observational error on each measurement is held constant at  $\delta m = 0.05$  throughout.

The uncertainties in the measured values of  $\alpha$  and  $t_1$  are strongly correlated. The slope of the correlation can be estimated easily by noting that

$$\frac{d \log f}{dt} = \frac{-\alpha}{\hat{t} + t_1} . \quad (1)$$

This implies that the expected error  $\delta t_1 \approx -\delta\alpha/(d \log f/dt)$ , where we can evaluate the observable quantity  $d \log f/dt$  near the midpoint of the observations.

#### 4. The Distribution of Discovery Times

The age of an orphan afterglow at first discovery is a key factor in how well we can determine its decay slope. In this section we predict this distribution in a simple orphan afterglow model. Our derivation is closely analogous to the Nakar et al (2002) orphan rate calculation, and includes the approximation that GRB jets have a standard energy. In this model, the light curve of off axis

orphan afterglows assumes a standard form. The maximum time  $t_{max}(z, m)$  at which an orphan is detectable is then determined uniquely by the redshift  $z$  of the burst and the magnitude limit  $m$  of the observations. For completeness, we reproduce here the result of inverting equations 6–7 of NPG02:

$$\frac{t_{1,max}}{\text{day}} = \left\{ 460 \frac{g_0(p)}{g_0(2.2)} 10^{\frac{2.2-p}{4}} \epsilon_{e,-1}^{p-1} \epsilon_{B,-2}^{(p-2)/4} n_0^{-(p+2)/12} E_{0,50.7}^{(p+2)/3} \nu_{14.7}^{-p/2} (1+z)^{\frac{p+2}{2}} d_{L,28}^{-2} \frac{\mu\text{Jy}}{f_{min}} \right\}^{1/p} \quad (2)$$

for the case where  $\nu_c < \nu$ , and

$$\frac{t_{1,max}}{\text{day}} = \left\{ 170 \frac{g_1(p)}{g_1(2.2)} 10^{\frac{2.2-p}{4}} \epsilon_{e,-1}^{p-1} \epsilon_{B,-2}^{(p+1)/4} n_0^{(3-p)/12} E_{0,50.7}^{(p+3)/3} \nu_{14.7}^{(1-p)/2} (1+z)^{\frac{p+3}{2}} d_{L,28}^{-2} \frac{\mu\text{Jy}}{f_{min}} \right\}^{1/p} \quad (3)$$

for the case  $\nu_c > \nu$ . Quantities in these equations are scaled to dimensionless or cgs unit values whose logarithms are indicated in the subscripts:  $p$  is the slope of the power law distribution of energies for electrons accelerated in the forward shock of the expanding GRB remnant;  $\epsilon_{e,-1}$  and  $\epsilon_{B,-2}$  are the fractions of internal energy going into relativistic electrons and magnetic fields at this shock, scaled to units of 0.1 and 0.01 respectively;  $n_0$  is the number density of the ambient medium;  $E_{0,50.7}$  is the initial kinetic energy of the ejecta in units of  $10^{50.7}$  erg,  $\nu_{14.7}$  is the observed frequency in units of  $10^{14.7}$  Hz,  $z$  is the GRB redshift, and  $d_{L,28}$  is the luminosity distance in units of  $10^{28}$  cm. The functions  $g_0(p) = 10^{-0.56p}(p - 0.98)[(p - 2)/(p - 1)]^{p-1}$  and  $g_1(p) = 10^{-0.31p}(p - 0.04)[(p - 2)/(p - 1)]^{p-1}$  vary slowly with  $p$  for  $p \gtrsim 2.2$  but become undefined for  $p \leq 2$ , since the assumed physical model for the radiating electron population gives a divergent total electron energy if  $p \leq 2$ .

An interesting feature of  $t_{1,max}$  is that it declines extremely slowly at high redshifts.  $t_{1,max}(z, m)$  is plotted for a few values of  $m$  in figure 3. Because our calculation of  $t_{1,max}$  has assumed the “universal” light curve for an off-axis jet, it is only valid for  $t_{1,max} > t_{jet}$ . We therefore overplot  $t_{jet,obs}$  for rest-frame  $t_{jet} = 0.7$  day.

Consider first the distribution of “turn-on time”<sup>2</sup>  $t_{on}$  under the approximation that the afterglow becomes visible when  $\theta_{obs} = 1/\Gamma$ . In the late time evolution of a spreading GRB jet,  $\Gamma \propto t^{-1/2}$  (Rhoads 1997, 1999). The distribution of off-axis angles should go as  $dN_{GRB}/d\theta_{obs} \propto \theta_{obs}$ . If we consider a single redshift and a single jet energy, we then obtain

$$\left( \frac{dN_{GRB}}{dt_{on}} \right)_{z,E_0} \propto \begin{cases} 1/(1+z) & \text{if } t_{jet} < t_{on} < t_{1,max}(z, E_0) \\ 0 & \text{otherwise} \end{cases} \quad (4)$$

Here  $N_{GRB}$  has units of events per day per unit volume, while  $\frac{dN_{GRB}}{dt_{on}}$  is in events per day<sup>2</sup> per unit volume. The factor of  $(1+z)^{-1}$  in the rate is required to account for cosmological time dilation of the observed turn-on time.

---

<sup>2</sup>The time at which an orphan afterglow could first be detected assuming continuous monitoring.

If we now assume a search strategy with observations regularly spaced at interval  $\delta t$ , the above distribution is modified to yield the distribution of age  $t_1$  at detection:

$$\left(\frac{dN_{GRB}}{dt_1}\right)_{z,E_0} \propto \begin{cases} \min(t_1/\delta t, 1)/(1+z) & \text{if } t_{jet} < t_1 < t_{1,max} \\ 0 & \text{otherwise} \end{cases} . \quad (5)$$

In the limit of continuous observations,  $\delta t \rightarrow 0$ , the two expressions become identical as required.

Now let us integrate over redshift. The rate of orphan detections per unit  $t_1$  becomes

$$R_{orph}(t_1) = \int_0^{z_{max}} \left(\frac{dN_{GRB}}{dt_1}\right)_{z,E_0} \frac{dV/dz}{1+z} dz \quad (6)$$

where  $m$  is the magnitude limit of the survey. Again following Nakar et al (2002), we take  $n(z)$  to grow as  $n(z) \propto 10^{0.75z}$  for  $z \leq 1$  and hold  $n(z)$  constant for  $z \geq 1$ . We fix the cosmology to currently fashionable values, i.e.,  $H_0 = 70 \text{ km s}^{-1} \text{ Mpc}^{-1}$ ,  $\Lambda_0 = 0.7$ ,  $\Omega_0 = 0.3$ . Numerical integration of  $R_{orph}(t_1)$  was done using the ‘‘Libcosm’’ C library (Yoshikawa 1999).

The overall GRB rate density was normalized to set the total on-axis GRB rate over the redshift range  $0 < z < 5$  to about 900 GRB/year, using a fixed rest-frame  $t_{jet} = 0.7$  day. This matches reasonably well the BATSE rate. A more accurate normalization may be impossible given present observational uncertainties. The shape of the  $t_1$  probability distribution is independent of the exact normalization of the GRB event rate.

Results of our numerical  $R_{orph}(t_1)$  calculations are shown in figure 4. A typical rate curve will show either three or four segments. The first is a rising segment, determined by the jet break time and the observational time sampling interval. The second is a ‘‘plateau’’ where  $R_{orph}(t_1)$  is essentially constant. This occurs when  $t_1$  exceeds both the sampling interval  $\delta t$  and the jet break time  $t_{jet}$ , and simultaneously the sensitivity of the survey is sufficient to detect orphans up to very high redshift. Such conditions are only met for comparatively sensitive surveys and short jet break times. The next segment is a falling one, whose typical time scale is determined by the magnitude limit of the survey. The last component is a low-level, late time tail comprised of the closest bursts, which can be detected at large angles off axis but over a very small volume.

We see that the peak of  $R_{orph}(t_1)$  occurs on times ranging from a couple of days to a couple of weeks, depending on the characteristic jet break time and the survey magnitude limit. Moreover, it can be quite sharply peaked for surveys of relatively bright flux limits ( $\sim 21$ st magnitude) but is rather broad for more sensitive surveys.

## 5. Implications for Orphan Afterglow Survey Strategy

I now outline an observing strategy for optical regime orphan afterglow surveys that incorporates the results of preceding sections together with earlier studies.



Monitoring should be carried out to a depth sufficient to find afterglows that are at least a few days old when their first photons reach the observer. Based on figure 4, this implies a depth of at least 23rd to 24th magnitude. Monitoring should also be carried out in multiple filters spanning at least the range  $400\text{nm} < \lambda < 800\text{nm}$ , in order to successfully separate afterglows from other transient events in a single epoch (Rhoads 2001). This will then allow followup observations to considerably greater depths, which may be needed as the event fades below the detection threshold of the original search. The search cadence for monitoring should be reasonably short,  $\delta t \lesssim t_{jet} \sim 1\text{day}$ , in order to distinguish jetlike events seen on-axis from other afterglows (see section 6).

Once a candidate has been identified, optical followup observations should proceed with a cadence scaled to the expected age of the event at first detection. For a search to 23rd magnitude, every 2 nights is probably sufficient, while shallower searches should be followed every night initially. Deeper searches might require only one or two samples per week. Such monitoring, pursued for half a dozen epochs (corresponding to a monitoring time  $\Delta t \gtrsim 2t_1$ ) would allow a sufficiently accurate measurement of the decay slope  $\alpha$  to distinguish between on- and off-axis events, despite the uncertainty in trigger time.

Each identified orphan afterglow candidate should also be observed twice or more at radio wavelengths. This will allow the test of section 2 to be applied and so distinguish between a laterally spreading jet and an on-axis dirty fireball.

Supplemental tests based on the nature of the transient’s host galaxy should also be applied, given the history of orphan afterglow searches so far. Some active galactic nuclei are capable of producing flares that closely resemble orphan afterglows, and indeed the first published optical orphan afterglow candidate (Vanden Berk et al 2002) turned out to be just such an event (Gal-Yam et al 2001). Such AGN flares can be separated from cosmological fireballs by long-term monitoring and/or spectroscopy of the host galaxy.

While the above strategy is observationally demanding, it should be within reach of already planned instruments. The ARAGO project (Boër 2001) will operate a transient search using a 1.5m telescope with a wide field ( $2 \times 2^\circ$ ) camera. Such a system will reach an interesting depth for off-axis orphan searches and may provide a few detections per year for followup with larger instruments. Further away but more powerful is the Large Synoptic Survey Telescope (LSST)<sup>3</sup>, which will survey about half the sky to a depth of  $\sim 24$  mag and a cadence of  $\sim 1$  week. Such a survey could discover hundreds of orphan afterglows per year. It would also provide real-time triggers, since multiple filters are planned. After a year or two of operation it would provide a good monitoring baseline for all afterglow candidates in its survey region, allowing comparatively easy rejection of some AGN. Finally, since the LSST will be an 8m class telescope, it would be capable of performing its own very deep followup observations, provided that enough flexibility in scheduling exists to spend extra integration time on interesting transients identified in the course

---

<sup>3</sup><http://www.lsst.org>

of the survey.

## 6. Discussion

It is likely that dirty fireballs, if they exist, are collimated by whatever mechanism collimates the gamma ray bursts. This raises the likelihood (discussed also by HDL02 and NPG02) that we will observe orphan afterglows due to off-axis dirty fireballs. It will be very difficult to determine whether any particular off-axis event emitted gamma rays. The best possibility here is to look for reprocessed radiation in some form, e.g., iron emission lines. Such reprocessed radiation may be substantially more isotropic than the synchrotron radiation from relativistic ejecta, and indeed has been proposed as a calorimeter of GRB energetics (Ghisellini et al 2002). Ghisellini et al point out that X-ray emission lines may still be anisotropic due to optical depth effects. Fortunately, the observation of an orphan afterglow implies that we are not terribly far from the jet axis. Observationally, searches for X-ray lines would require very rapid and sensitive X-ray followup of orphan afterglows discovered in ongoing variability surveys, given that the observed lifetime of all X-ray lines so far observed is  $\lesssim 2$  days and the typical time lag to observe an orphan is comparable. Additionally, X-ray lines only require photons sufficiently energetic to excite the iron K edge,  $\sim 7\text{keV}$ . Thus, while these lines would place an interesting constraint on the fireball Lorentz factor, they do not guarantee that an event produced gamma rays.

Predictions for orphan afterglows will also depend on the GRB jet profile, that is, the variation of ejecta Lorentz factor ( $\Gamma(\theta)$ ) and kinetic energy ( $dE/d\Omega(\theta)$ ) with the off-axis angle  $\theta$ . Our calculations in this paper have followed the expanding top-hat approximation, where both  $\Gamma$  and  $dE/d\Omega$  are step functions with some fixed value at  $\theta < \theta_j$ , dropping to zero at  $\theta > \theta_j$ . This is the best explored model for collimated GRB afterglows, including essentially all work on orphan afterglows to date. However, it remains an idealized case of more general and realistic jet models. The light curve breaks expected in an expanding top-hat case (Rhoads 1999) are expected also in cases where  $dE/d\Omega \propto \theta^{-k}$  with  $k \approx 2$ . However, in this case the break time indicates the observer’s off-axis angle  $\theta_{obs}$  instead of a jet opening angle  $\theta_j$  (Rossi et al 2002; Zhang & Mészáros 2002). Similarly, while orphan afterglows are a reasonable expectation in such “inhomogeneous” jets, the detailed predictions may change. If we allow  $dE/d\Omega$  to decline smoothly with  $\theta$  while holding  $\Gamma$  fixed, we expect most afterglows to be accompanied by  $\gamma$ -ray emission, since there are fast ejecta along the line of sight regardless of  $\theta_{obs}$ . On the other hand, if we fix  $dE/d\Omega$  and allow  $\Gamma$  to decline, we enter a regime where events viewed near the jet axis yield GRBs and those seen at larger angles behave as on-axis dirty fireballs. The fully general case (where both  $dE/d\Omega$  and  $\Gamma$  vary smoothly) may yield a range of behaviors between these limiting extremes.

A final complication is the need to correctly account for the population of conventional GRB afterglows in orphan afterglow searches. Limits to the sky coverage and sensitivity of GRB detectors imply that the  $\gamma$ -ray emission will go undetected in a substantial fraction of the conventional GRB afterglows discovered by any orphan search. Being on-axis, these events will generally show a slow

initial decay followed by a jet break. If the time sampling of the orphan survey is sufficiently dense ( $\delta t < t_{jet}$ ), these conventional afterglows will typically also be seen with brighter initial magnitude than off-axis orphans. Thus, they resemble the likely properties of a dirty fireball population, and the observational tests we have described will serve to distinguish them from off-axis orphans.

Confusion between conventional GRBs and dirty fireball populations remains possible. To remove this confusion, the expected rate of conventional afterglows in an orphan survey could be calculated using the known  $\gamma$ -ray and afterglow properties of conventional GRBs. An accurate correction might be difficult at present, because the ratio of afterglow to  $\gamma$ -ray flux shows a wide dispersion and because the data in currently available samples are very heterogeneous. Fortunately, more homogeneous and statistically tractable samples should become available with the launch of the Swift mission.

Swift offers another potential way to mitigate confusion by conventional GRBs: Orphan searches could be conducted preferentially in regions monitored by the Swift Burst Alert Telescope (BAT). With a set of  $\sim 10$ – $20$  fields evenly spaced on the sky, at least one would always fall within the 2 steradian field of the BAT. The BAT duty cycle at any point on the sky is limited by Earth occultation to  $\lesssim 50\%$ , with each continuous observation  $\lesssim 50$  minutes. For each orphan search field, the number of afterglows with Swift counterparts could be counted, and the total number of conventional afterglows in the sample could then be inferred by a simple correction for the Swift duty cycle. This correction could be fairly precisely derived using the known Swift pointing history, and would a factor between 2 and 10.

On-axis orphan searches could be performed with a much wider field, brighter flux limit, and faster observing cadence than the off-axis searches we have primarily considered here (Nakar & Piran 2002). Such surveys are natural successors to current robotic telephoto lens projects (e.g., Kehoe et al 2002). In this limit, it would be possible to *always* monitor fields in the BAT field of view, and thereby know whether any particular optical flash was or was not accompanied by a GRB. Implementing this strategy would require switching fields approximately twice per Swift orbit (assuming Swift changes targets to avoid Earth occultation), and would require real-time knowledge of the Swift pointing, but neither of these should be an insurmountable difficulty.

A general and robust orphan search strategy is to require sufficient areal and time coverage to ensure the detection of some conventional GRB afterglows, and hence also of on-axis dirty fireballs from any population with an event rate comparable to the GRB rate. The search cadence should be kept at  $\delta t \lesssim t_{jet}$  (suggesting nightly observations) in order to catch the on-axis orphans before their jet break and so recognize them. If such coverage fails to find on axis orphans, it will mean that dirty fireballs do not contribute substantially to the overall orphan afterglow rate. More probably, we will find on-axis orphans. Comparing their rate to the GRB rate will tell us the fraction of cosmological fireballs that achieves  $\Gamma_0 \gtrsim 100$ . A large class of dirty fireballs might be found, and if it is, would tell us that GRBs are a minority population in a much larger class of cosmological fireballs. The combined knowledge of the on-axis dirty fireball rate and the off-axis orphan rate

would then allow correction of the orphan statistics for dirty fireballs, and lead to the desired constraint on GRB collimation from orphan counts.

I thank an anonymous referee for useful comments that strengthened this paper. This research was partially supported by an Institute Fellowship at The Space Telescope Science Institute (STScI).

## REFERENCES

- Akerlof, C. et al 1999, *Nature* 398, 400
- Boër, M., 2001, *Astronomische Nachrichten* 322, 343
- Chevalier, R., & Li, Z.-Y. 1999, *ApJ* 520, L29
- Chevalier, R., & Li, Z.-Y. 2000, *ApJ* 536, 195
- Dalal, N., Griest, K., & Pruet, J. 2002, *ApJ* 564, 209
- Frail, D. A., et al 2001, *ApJ* 562, L55
- Gal-Yam, A., Ofek, E. O., Filippenko, A. V., Chornock, R., & Li, W. 2002, *PASP* 114, 587
- Ghisellini, G., Lazzati, D., Rossi, E. M., & Rees, M. J. 2002, accepted to *A&A*, astro-ph/0205227
- Goodman, J. 1986, *ApJ* 308, L47
- Granot, J., Panaitescu, A., Kumar, P., & Woosley, S. E. 2002, *ApJ* 570, 61
- Heise, J., in 't Zand, J., Kippen, M., & Woods, P. 2001, astro-ph/0111246
- Huang, Y. F., Dai, Z. G., & Lu, T. 2002, *MNRAS* 332, 735 (HDL02)
- Kehoe, R., et al 2002, *ApJ* 577, 845
- Krolik, J. H., & Pier, E. A. 1991, *ApJ* 373, 277
- Nakar, E., Piran, T., & Granot, J. 2002, astro-ph/0204203 (NPG02)
- Nakar, E., & Piran, T. 2002, *NewA*, submitted, astro-ph/0207400
- Paczyński, B. 1986, *ApJ* 308, L43
- Panaitescu, A., & Kumar, P. 2002, *ApJ* 571, 779
- Rhoads, J. E. 1997, *ApJ* 487, L1
- Rhoads, J. E. 1999, *ApJ* 525, 737
- Rhoads, J. E. 2000, proceedings of the 9th Marcel Grossmann Meeting, astro-ph/0103028
- Rhoads, J. E. 2001, *ApJ* 557, 943
- Rossi, E., Lazzati, D., Rees, M. J., 2002, *MNRAS* 332, 945
- Sari, R., Piran, T., & Narayan, R. 1998, *ApJ* 497, L17

- Sari, R., Piran, T., & Halpern, J. 1999, ApJ 519, L17
- Totani, T., & Panaitescu, A. 2002, ApJ in press, astro-ph/0204258
- Vanden Berk, D. E., et al 2002, ApJ 576, 673
- Woods, E., & Loeb, A. 1995, ApJ 453, 583
- Yoshikawa, K. 1999, “Libcosm” C program library,  
see <http://www.kusastro.kyoto-u.ac.jp/~kohji/research/libcosm>
- Zhang, B., & Mészáros, P. 2002, ApJ 571, 876

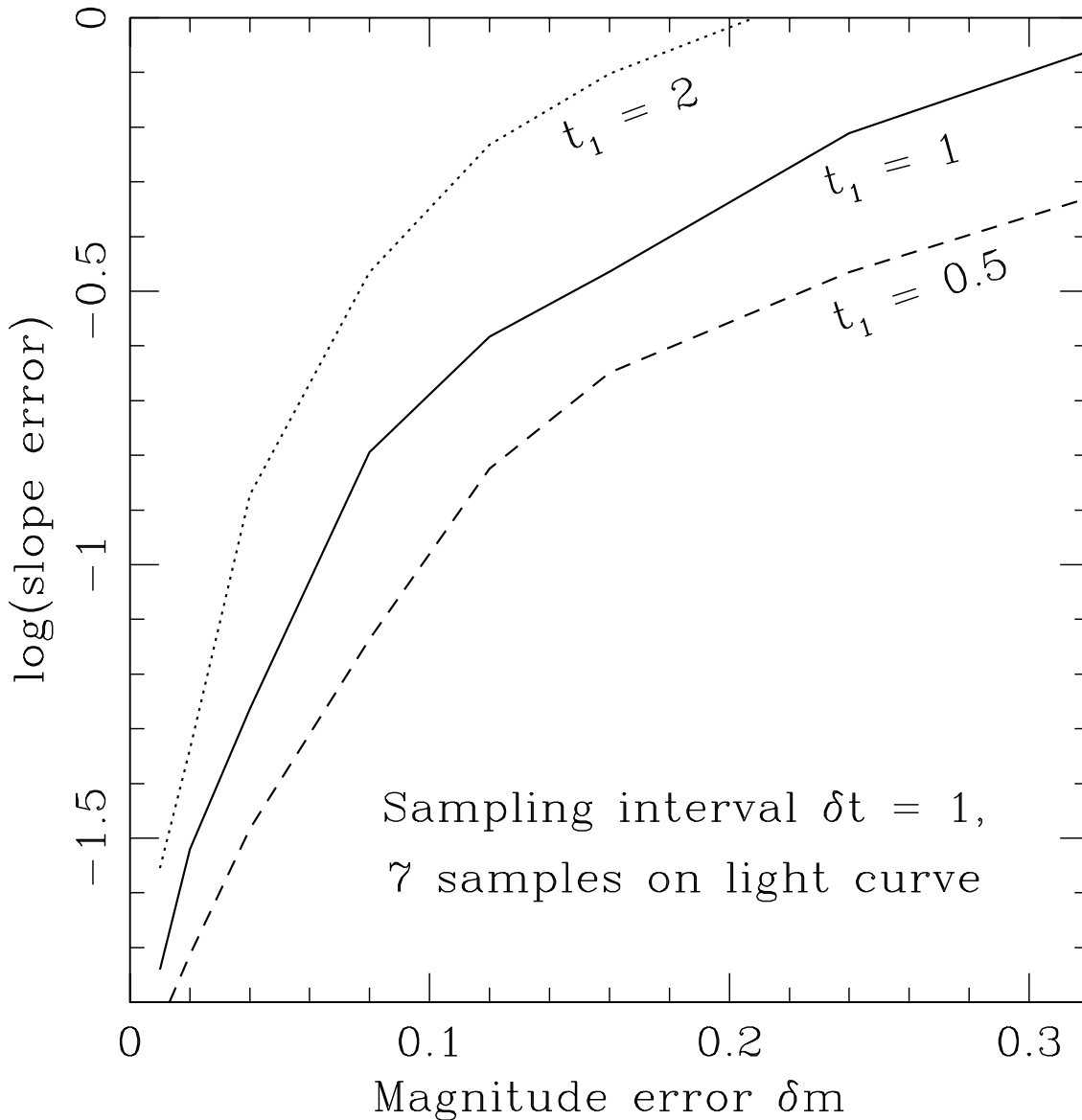


Fig. 1.— The error in the measured light curve decay slope for an orphan afterglow. The decay is taken to be a pure power law with an unknown time origin that is fitted as a parameter of the model. Curves are shown for three different ages of the event at the time of first observation. Observations are assumed at 1 day intervals continuing for 7 observations in total. All observations are assumed to have the same logarithmic flux error, which is plotted in magnitude units on the  $x$ -axis. The resulting error in inferred slope, shown on the  $y$ -axis, is derived by Monte Carlo simulations of a least squares fitting procedure to the light curve. A logarithmic slope error of  $-0.5$  is approximately sufficient to distinguish orphan afterglows produced by on-axis dirty fireballs from those produced by off-axis gamma ray bursts.

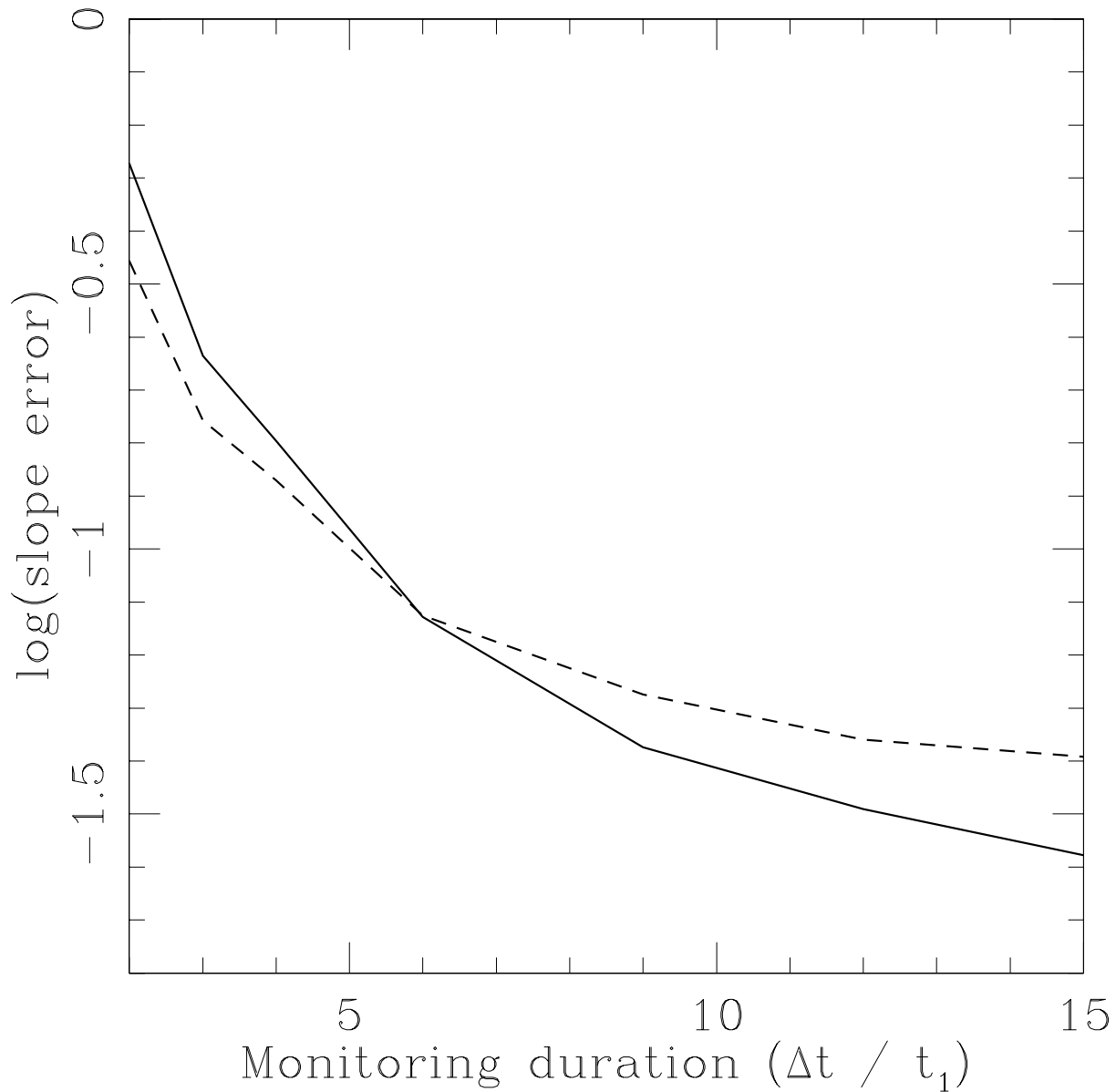


Fig. 2.— The error in the light curve decay slope as a function of the monitoring campaign duration. The solid line shows the result if the number of samples is varied and the interval remains fixed (with  $\delta t = t_1$ ). The dotted curve shows the result for a fixed number of data points ( $N = 7$ ) and a varying  $\delta t$ . The flux error on each measurement is taken to be  $\delta m = 0.05$  for both curves.

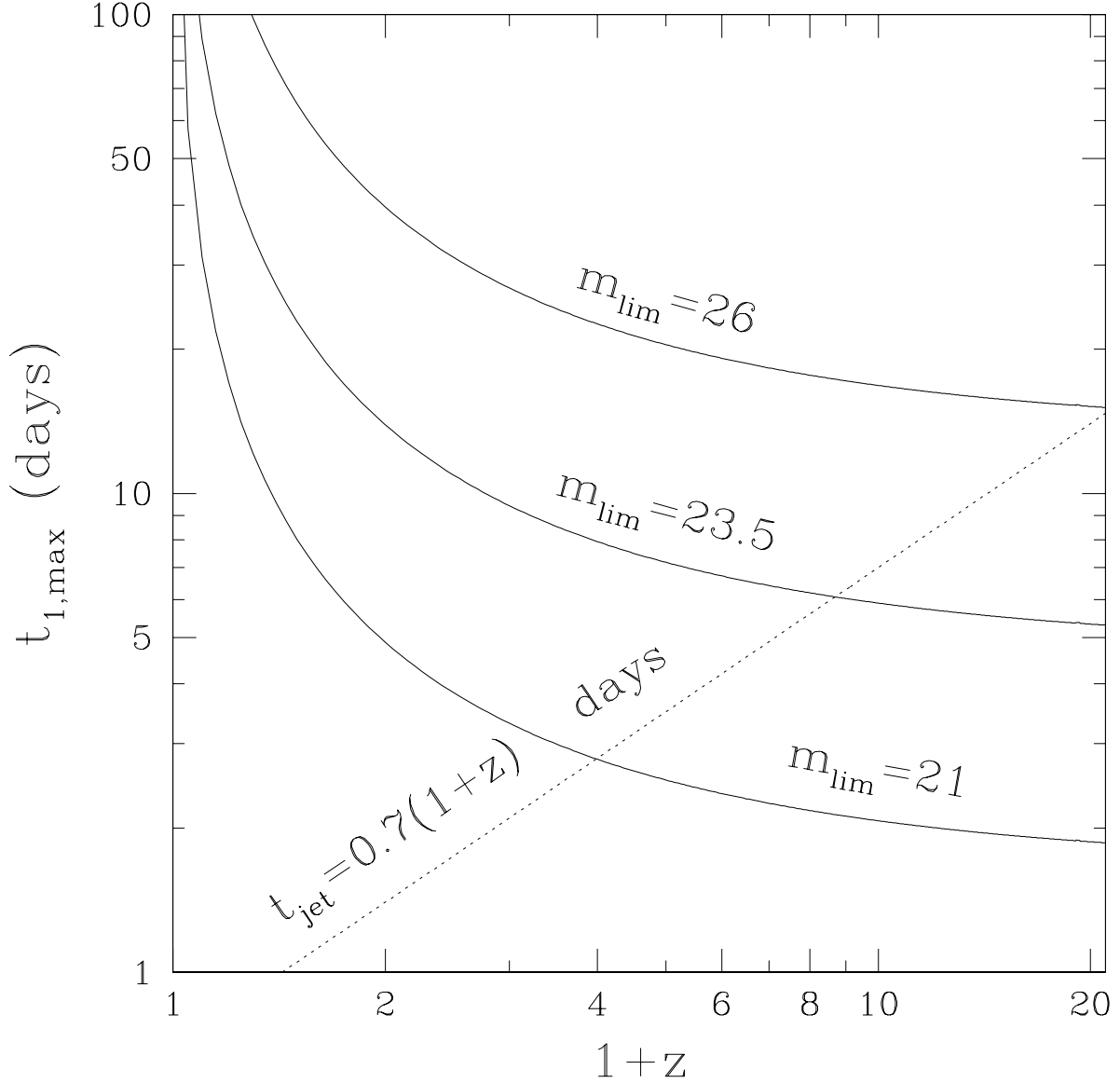


Fig. 3.— The maximum age at which an afterglow could be detected as a function of redshift, for three different survey flux thresholds. The light curve assumed is the “universal” late time light curve of an off axis jet, and the plotted curves are therefore not meaningful for values of  $t_{1,\max} < t_{\text{jet}}$ . The fluxes are derived from equation 2, with all physical parameters of the fireball held at their fiducial values, so that  $t_{1,\max} = \left[ (1+z)^{\frac{p+2}{2}} d_{L,28}^{-2} \left( \frac{460 \mu\text{Jy}}{f_{\text{min}}} \right) \right]^{1/p}$  with  $p = 2.2$ .



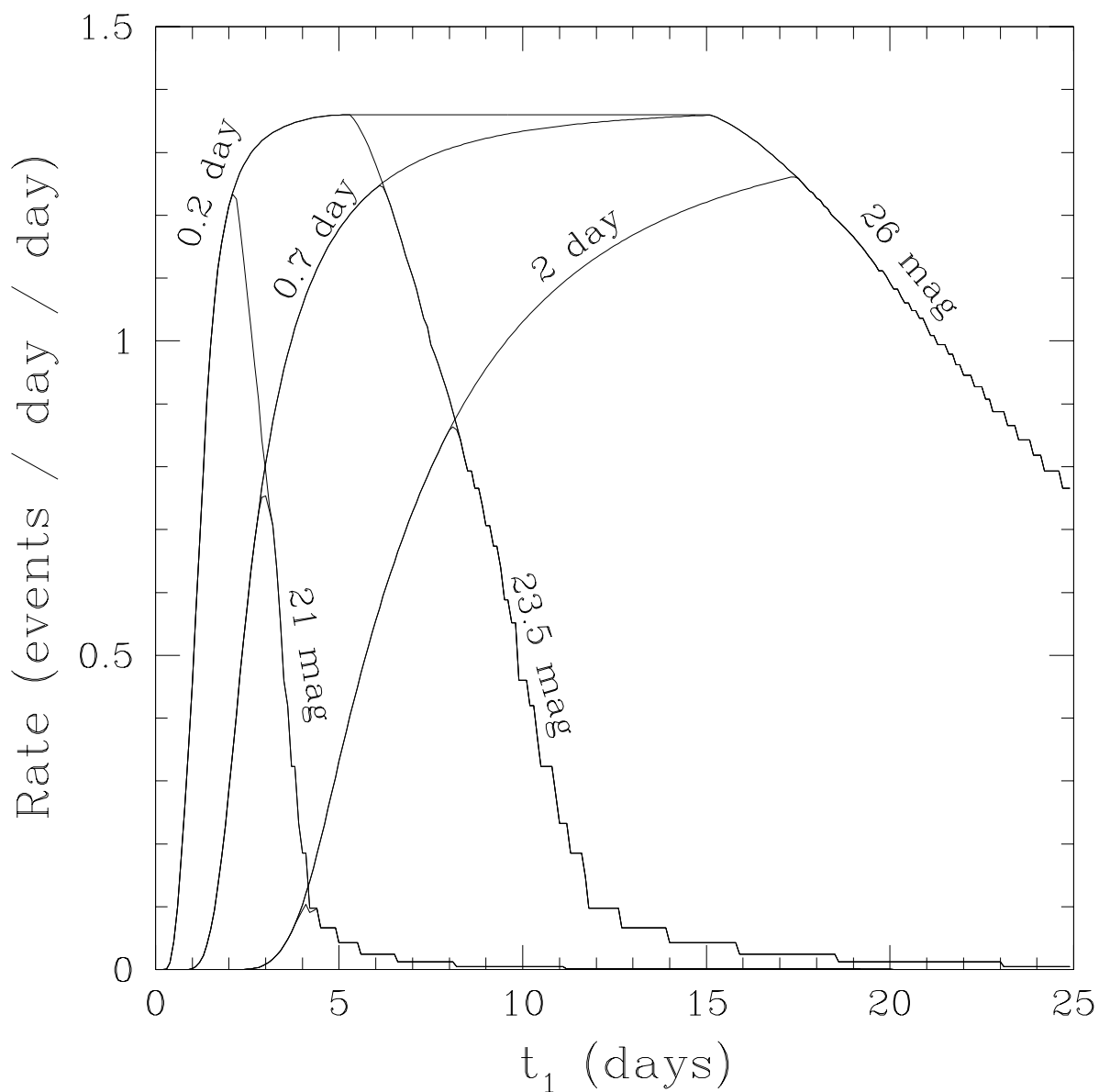


Fig. 4.— Distributions of orphan afterglow age at the time of first detection for spreading jet models with a range of jet break times and monitoring programs. The rising part of each curve is effectively set by the jet break time (marked on each curve) and the light curve sampling interval (here fixed at 1 day). The declining part of each curve is effectively set by the magnitude limit of the survey.